Journal of Zhejiang University-SCIENCE B (Biomedicine & Biotechnology)
ISSN 1673-1581 (Print); ISSN 1862-1783 (Online)
www.zju.edu.cn/jzus; www.springerlink.com
E-mail: jzus@zju.edu.cn

Multilayered polyelectrolyte-coated gold nanorods as multifunctional optical contrast agents for cancer cell imaging*

Li-li CHEN[1], Li JIANG[1], Ya-lun WANG[1], Jun QIAN[†‡1], Sailing HE[1,2]

([1]*Centre for Optical and Electromagnetic Research, State Key Laboratory of Modern Optical Instrumentation, Zhejiang University, Hangzhou 310058, China*)

([2]*Department of Electromagnetic Engineering, School of Electrical Engineering, Royal Institute of Technology, S-100 44 Stockholm, Sweden*)

[†]E-mail: qianjun@coer.zju.edu.cn

Received Nov. 27, 2009; Revision accepted Mar. 9, 2010; Crosschecked May 6, 2010

Abstract: We report the application of multilayered polyelectrolyte-coated gold nanorods (GNRs) as multifunctional optical contrast agents for cancer cell imaging. The surface modification of GNRs improves their chemical stability and facilitates them to be taken up by cancer cells through electrostatic interaction. The unique longitudinal surface plasmon resonance property of GNRs makes them suitable as both "scattering contrast agents" and "Raman contrast agents". In our experiments, the staining of GNRs in cells was further confirmed by dark field microscopy and Raman microscopy. Our experiment results indicated that GNRs have great potential as multifunctional "optical contrast agents" for future in vivo animal imaging.

Key words: Gold nanorods, Polyelectrolyte, Scattering, Raman, Cancer cell imaging
doi:10.1631/jzus.B0910731 **Document code:** A **CLC number:** Q2; TN2; R73

1 Introduction

Gold nanorod (GNR), which is a new-style of gold nanoparticles with rod structure, has been widely applied in bio-photonics research due to their unique optical properties (Perez-Juste *et al*., 2005). GNR has two surface plasmon resonance (SPR) bands. One is called a longitudinal band, which corresponds to electron oscillation along the long axis of GNRs, and the other is called a transverse peak, which corresponds to electron oscillation along the short axis of GNRs. The transverse extinction band is usually around 520 nm, while the longitudinal extinction band can be tuned from the visible to the near-infrared (600–900 nm, which is usually considered as an optical window of biological tissue) by adjusting the aspect ratio (length divided by width) of GNR (Link *et al*., 1999; Huang *et al*., 2006).

The longitudinal SPR extinction of GNRs is composed of scattering and absorption, and according to the Mie scattering theory (Jain *et al*., 2006), the ratio of scattering in the total extinction depends on both the effective radius r_{eff} and the aspect ratio of GNRs. Based on their scattering property, GNRs can be utilized as "scattering contrast agents" for dark field imaging of cells (Ding *et al*., 2007; Oyelere *et al*., 2007; Yu *et al*., 2007a; 2007b; Hu *et al*., 2009; Lee *et al*., 2009).

The longitudinal SPR characteristic of GNRs also makes them suitable for the application of surface enhanced Raman scatting (SERS) (Orendorff *et al*., 2006). Raman signal is a fingerprint spectrum used to characterize molecule structure. It is usually too weak, however, to be detected. GNRs have a strong surface localized electromagnetic field, and it can be used to enhance the Raman scattering intensity

‡ Corresponding author

* Project supported by the Swedish Foundation for Strategic Research (SSF) and the US Air Force Office of Scientific Research (Asia Office)

of molecules, which are adsorbed on GNRs surfaces, up to 10^{14}-fold (Camden *et al*., 2008). Based on this characteristic, molecule (rich of Raman scattering information)-coated GNRs can be used as "Raman contrast agents" (Huang *et al*., 2007; Oyelere *et al*., 2007; von Maltzahn *et al*., 2009) for both in vitro and in vivo bio-imaging.

In our demonstrated work, as-synthesized GNRs were encapsulated with two layers of polyelectrolytes. The first layer is called poly-styrene sulfonate (PSS), which is negatively charged and rich of Raman information, and the second layer is called poly-allylamine hydrochloride (PAH), which is positively charged (Pastoriza-Santos *et al*., 2006). The PAH-PSS-GNRs carried net positive charges and could stain cancer cells due to the electrostatic interaction. Through both dark field microscopy and Raman microscopy, the uptake of multilayered polyelectrolyte-coated GNRs in cancer cells was confirmed, based on their unique scattering property and SERS effect. Our experiment results indicated that GNRs have great potentials to be applied as multifunctional "optical contrast agents" for future in vivo animal imaging.

2 Materials and methods

GNRs used in our experiment were synthesized by a two-step seed-mediated growth method, which has been fully reported by our group before (Li *et al*., 2008). The as-synthesized GNRs were then centrifugated twice to remove the excess cetyltrimethyl ammonium bromide (CTAB) molecules and then redispersed in 12.5 ml deionized water. The procedure of coating GNRs with multilayered polyelectrolytes is shown in Fig. 1. Briefly, 0.25 ml GNRs solution, 200 μl PSS (210 mg/ml in aqueous solution), and 100 μl of 30 mmol/L NaCl solution were added into 0.75 ml deionized water, and the mixed solution was then vortexed vigorously for 3 min. After 3 h adsorption time, the excess PSS molecules in the supernatant fraction were removed by centrifugation twice, and the pellet was redispersed in 1 ml deionized water. For PAH coating, 200 μl PAH solution (10 mg/ml in 10 mmol/L NaCl) and 100 μl of 10 mmol/L NaCl solution were added into 1 ml PSS-GNRs solution, and the mixed solution was then vortexed vigorously for 3 min. After 3-h adsorption time, the excess PAH molecules in the supernatant fraction were removed by centrifugation twice, and the pellet was redispersed in 1 ml deionized water. The obtained PAH-PSS-GNRs could be then used for further cell imaging experiment.

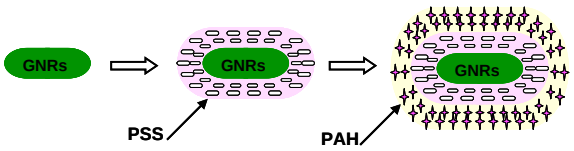

Fig. 1 Schematic diagram illustrating multilayered polyelectrolyte functionalization of GNRs

Transmission electron microscope (TEM) picture of GNRs was taken by a JEOL JEM-1200EX TEM (Japan). Ultraviolet-visible (UV-vis) absorbance spectrum was recorded by a Shimadzu 2550 UV-vis scanning spectrophotometer (Japan). Zeta potential measurements were performed on a Malvern Zetasizer Nano ZS90 instrument (UK) at room temperature. Raman spectrum of GNRs solution was measured by a Raman probe system (Ocean Optics, USA), in which a 785-nm laser (max power 300 mW) and a Raman spectrophotometer were adopted.

HeLa cells (human cancer cell lines) were cultivated in Dulbecco minimum essential media (DMEM) with 10% (w/v) fetal bovine serum (FBS), 1% (w/v) penicillin, and 1% (w/v) amphotericin B. One day before the treatment, cells were seeded in 35-mm glass cultivation dishes at a confluence of 70%–80%. During the treatment, different samples (40 μl CTAB-GNRs, PSS-GNRs, and PAH-PSS-GNRs with concentration of 13.1 pmol/ml) were separately added to the cell plates and the cell incubation process lasted for 2 h at 37 °C with 5% CO_2. Then the cells were washed thrice with phosphate buffered saline (PBS) and directly imaged with a Nikon Eclipse ME600 microscope (Japan) with a dark field condenser (oil immersion type, with a numerical aperture between 1.2 and 1.43) and an objective lens (50×/numerical aperture (NA) 0.55). For Raman imaging, cells were cultivated in glass slides. After sample treatment and PBS washing, cells were fixed and the glass slide was covered by cover-glass. The treated cells were then imaged with an inVia Reflex Raman spectra microscope (Renishaw Ltd., UK).

3 Results and discussion

Fig. 2b shows the TEM picture of our synthesized GNRs. As we can see, GNRs were of rod shapes and their sizes were very mono-distributed. Besides, the yield efficiency of GNRs was very high, and almost no nanoparticles with other shapes could be observed. According to the extinction spectrum (Fig. 2c), the as-synthesized GNRs have two SPR peak. The transverse extinction peak is around 520 nm while the longitudinal extinction peak is around 636 nm. Under the daylight lamp (white light), GNRs solution took on green color (Fig. 2a).

According to the TEM picture, the average diameter and length of GNRs could be measured and calculated. The average diameter and length of GNRs are 25 nm and 55 nm, respectively. Based on these data and discrete dipole approximation (DDA) calculation method (Kim *et al*., 2009), the simulated extinction spectrum of our synthesized GNRs could also be obtained (Fig. 3). The extinction spectrum was further divided into absorption and scattering. According to the Mie scattering theory, since the effective radius r_{eff} (the GNR volume $V_{\text{GNR}}=4\pi r_{\text{eff}}^3/3$) of the GNRs was not so big, scattering occupied the minority of the longitudinal extinction. The scattering intensity of GNRs, however, was still high enough for dark field scattering imaging, and the GNRs should scatter red light under the white irritation, since the simulated scattering peak wavelength was 640 nm. Another interesting phenomenon is that there is almost no scattering occupied in transverse extinction, which means that the transverse extinction is mostly caused by absorption effect.

As shown in Fig. 4a, after PSS coating, the absorption peak of GNRs has a 2-nm red-shift of the longitudinal SPR band (638 nm). After PAH coating, the absorption peak of GNRs has another 0.5-nm red-shift of the longitudinal SPR band (638.5 nm). Furthermore, the absorption spectra of GNRs do not show obvious broadening related to the aggregation of nanorod particles. The surface charge properties of CTAB-GNRs, PSS-GNRs, and PAH-PSS-GNRs were also characterized through Zeta potential measurements. As shown in Fig. 4b, CTAB-GNRs, PSS-GNRs, and PAH-PSS-GNRs carried positive charge (+28.2 mV), negative charge (−35.5 mV), and positive charge (+43.9 mV), respectively. Multilayered polyelectrolyte coating could reduce the aggregation of GNRs in solution, and it could also make GNRs more chemically stable and less toxic in bio-environment. Furthermore, the net positive charges on PAH-PSS-GNRs surfaces could make them to be more readily taken up by cells due to the electrostatic interaction.

Different GNRs samples were used for in vitro cancer cell imaging with dark field microscopy, and HeLa cell lines were chosen as the target cells. Fig. 5a is the dark field imaging of HeLa cells without any treatment. Under the white light irritation, HeLa cells scattered blue light, and their nucleus could be easily discriminated from their cell cytoplasm. This phenomenon is very difficult to observe under common transmission microscopy, and it indicates that dark field microscopy can provide details with higher contrast rather than common transmission microscopy. Fig. 5c illustrates the similar result with Fig. 5a, and almost no red light (scattered from GNRs) could be observed. Since cell membranes usually carry negative charge, PSS-GNRs (also negatively charged) would be “repelled” from cells surfaces, and they could not have been taken up by cells. CTAB-GNRs carried positive charge, but they were not so stable, and they were prone to aggregating in the DMEM solution quickly. As shown in Fig. 5b, after the treatment of CTAB-GNRs, there was still no red light covering cancer cells, but some big red spots (aggregates of GNRs) could be observed outside the cells. Compared with CTAB-GNRs, PAH-PSS-GNRs also carried positive charge, but the multilayered polyelectrolyte coating could effectively prevent GNRs from aggregating and keep them chemically stable in various bio-environments. As shown in Fig. 5d, HeLa cells treated with PAH-PSS-GNRs emitted red light, and it was due to the light scattering (illustrated by Fig. 3) of GNRs, which covered the cell surfaces. The uptake is mediated through the electrostatic interaction between the positive charge on GNRs and negative charge on cell membranes.

Raman spectra of different GNRs samples (in aqueous solution) were measured by a Raman probe system (Ocean Optics). A 785-nm diode laser (300 mW) was used to excite samples, since this wavelength locates in the optical window of biological tissue (700–900 nm), and it could also eliminate fluorescence noise greatly. The integration time

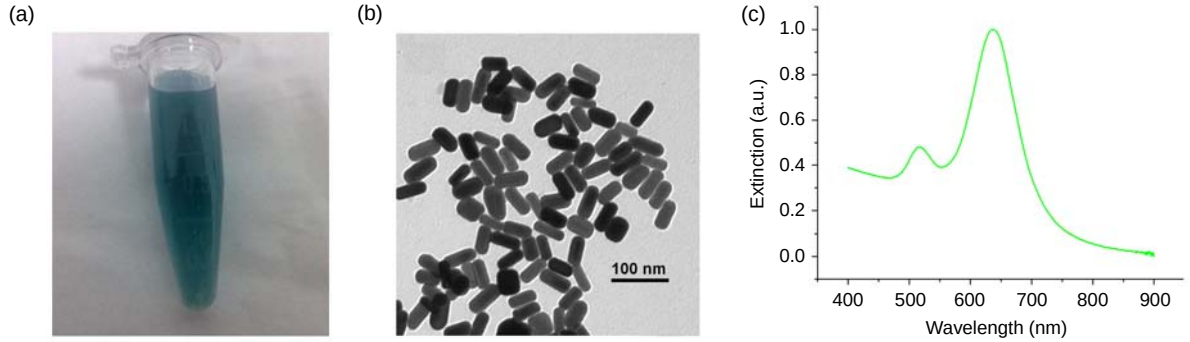

Fig. 2 (a) Photograph of GNRs aqueous solution; TEM image (b) and extinction spectrum (c) of as-synthesized GNRs

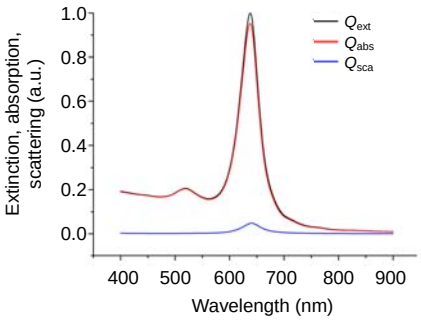

Fig. 3 Simulated extinction (Q_{ext}), absorption (Q_{abs}), and scattering (Q_{sca}) spectra of our synthesized GNRs

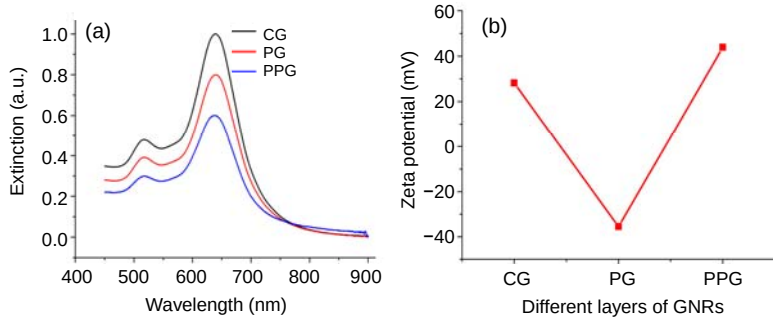

Fig. 4 Extinction spectra (a) and Zeta potential (b) data of CTAB-coated, PSS-capped and PAH-PSS-capped GNRs
CG: CTAB-GNRs; PG: PSS-GNRs; PPG: PAH-PSS-GNRs

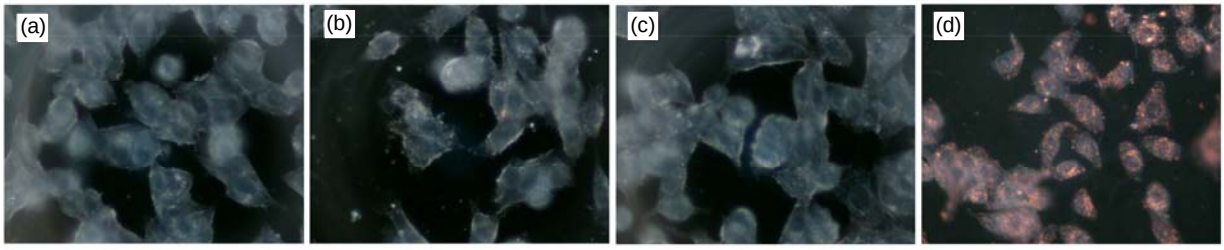

Fig. 5 Dark field images of HeLa cells without treatment (a), with CTAB-GNRs treatment (b), with PSS-GNRs treatment (c), and with PAH-PSS-GNRs treatment (d)

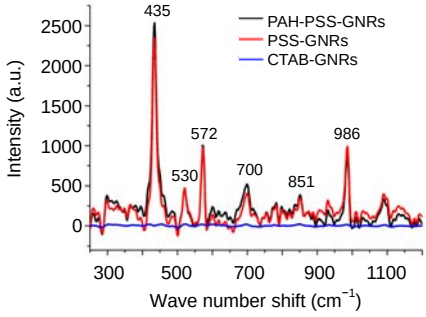

Fig. 6 Raman spectra of CTAB-GNRs, PSS-GNRs, and PAH-PSS-GNRs solution
The characteristic Raman peaks of PSS are located at 435, 530, 572, 700, 851, and 986 cm^{-1}

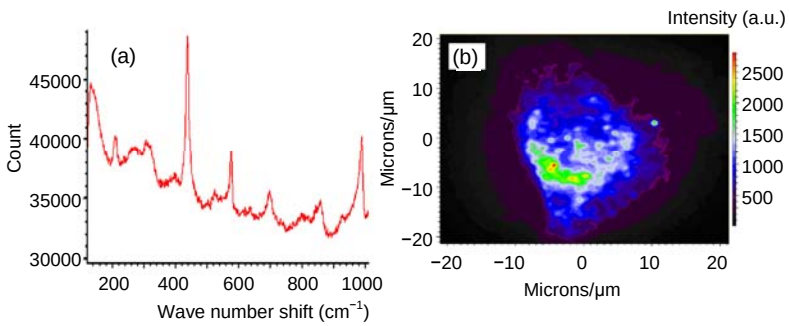

Fig. 7 (a) Raman spectrum of HeLa cells treated with PAH-PSS-GNRs; (b) Raman spectrum mapping of single HeLa cell treated with PAH-PSS-GNRs (435 cm^{-1} was set as the standard peak)

of the detector was 40000 ms. As shown in Fig. 6, CTAB-GNRs had no characteristic Raman peaks. PSS-GNRs had several distinct characteristic Raman peaks, however, which located in 435, 572 and 986 cm^{-1}. Some small peaks, like 530, 700 and 851 cm^{-1}, could also be observed. All the peaks arose from the SERS of PSS molecules, which are adsorbed on the surfaces of GNRs. PAH-PSS-GNRs had the similar Raman spectrum with that of PSS-GNRs, indicating that the SERS effect of PAH was not so intense and the SERS signal of PSS occupied majority in the whole PAH-PSS-GNRs system.

HeLa cell treated with PAH-PSS-GNRs was further imaged with Raman microscope (inVia Reflex, Renishaw Ltd.), and the wavelength of excitation laser was also set at 785 nm. Fig. 7a shows the Raman spectrum from the surfaces of HeLa cells, which were fully covered by PAH-PSS-GNRs (Fig. 5d). Compared with the Raman spectrum of PAH-PSS-GNRs solution, although the 530 cm^{-1} peak seemed a bit compressed, the Raman peaks at 435, 572 and 986 cm^{-1} were still very distinct and the 700 and 851 cm^{-1} peaks also became more obvious. Furthermore, fast Raman imaging was carried out by utilizing 435 cm^{-1} peak as the standard peak, and the Raman spectrum mapping on cell surface was obtained accordingly (Fig. 7b). Since only PAH-PSS-GNRs have the characteristic peak at 435 cm^{-1}, the Raman mapping could also reveal the distribution of PAH-PSS-GNRs on cell surface. Different mapping signal colors stand for different Raman intensities at different locations, and some high intensity spots (red, >2500 a.u.) could also reveal the local small aggregation of GNRs, since aggregation of GNRs increased the number of "hot spots", which could greatly increase the SERS signal. The cell Raman imaging results proved that PAH-PSS-GNRs could also be used as "Raman contrast agents" for cancer cell staining.

4 Conclusions

Multilayered polyelectrolyte-coated GNRs, which carried positive charge and were very stable in bio-environments, were obtained through facile chemical methods. Based on their unique scattering property and SERS effect, both dark field microscopy and Raman microscopy were used to confirm the uptake of multilayered polyelectrolyte-coated GNRs in cancer cells through the electrostatic interaction. The experiment results indicate that GNRs can be effectively used as multifunctional "optical contrast agents" for in vitro cancer cell imaging.

5 Acknowledgement

The authors are very grateful to Prof. Lian-kun DAI (Zhejiang University, China) for his help in Raman spectrum measurement. We also appreciate Mr. Chun-jian MIAO and Dr. Bao-kun HUANG (Renishaw Ltd., UK) for their help in Raman imaging.

References

Camden, J.P., Dieringer, J.A., Wang, Y.M., Masiello, D.J., Marks, L.D., Schatz, G.C., Van-Duyne, R.P., 2008. Probing the structure of single-molecule surface-enhanced Raman scattering hot spots. *Journal of the American Chemical Society*, **130**(38):12616-12617. [doi:10.1021/ja8051427]

Ding, H., Yong, K.T., Roy, I., Pudawar, H.E., Law, W.C., Bergey, E.J., Prasad, P.N., 2007. Gold nanorods coated with multilayer polyelectrolyte as contrast agents for multimodal imaging. *Journal of Physical Chemistry C*, **111**(34):12552-12557. [doi:10.1021/jp0733419]

Hu, R., Yong, K., Roy, I., Ding, H., He, S., Prasad, P.N., 2009. Metallic nanostructures as localized plasmon resonance enhanced scattering probes for multiplex dark-field targeted imaging of cancer cells. *The Journal of Physical Chemistry C*, **113**(7):2676-2684. [doi:10.1021/jp8076672]

Huang, X.H., El-Sayed, I.H., Qian, W., El-Sayed, M.A., 2006. Cancer cell imaging and photothermal therapy in the near-infrared region by using gold nanorods. *Journal of the American Chemical Society*, **128**(6):2115-2120. [doi:10.1021/ja057254a]

Huang, X.H., El-Sayed, I.H., Qian, W., El-Sayed, M.A., 2007. Cancer cells assemble and align gold nanorods conjugated to antibodies to produce highly enhanced, sharp, and polarized surface raman spectra: a potential cancer diagnostic marker. *Nano Letters*, **7**(6):1591-1597. [doi:10.1021/nl070472c]

Jain, P.K., Lee, K.S., El-Sayed, I.H., El-Sayed, M.A., 2006. Calculated absorption and scattering properties of gold nanoparticles of different size, shape, and composition: Applications in biological imaging and biomedicine. *Journal of Physical Chemistry B*, **110**(14):7238-7248. [doi:10.1021/jp057170o]

Kim, S., Jung, Y., Gu, G.H., Suh, J.S., Park, S.M., Ryu, S., 2009. Discrete dipole approximation calculations of optical properties of silver nanorod arrays in porous anodic alumina. *Journal of Physical Chemistry C*, **113**(37):16321-16328. [doi:10.1021/jp811516s]

Lee, S.E., Sasaki, D.Y., Perroud, T.D., Yoo, D., Patel, K.D., Lee, L.P., 2009. Biologically functional cationic phospholipid-gold nanoplasmonic carriers of RNA. *Journal of the American Chemical Society*, **131**(39):14066-14074. [doi:10.1021/ja904326j]

Li, X., Qian, J., He, S.L., 2008. Impact of the self-assembly of multilayer polyelectrolyte functionalized gold nanorods and its application to biosensing. *Nanotechnology*, **19**(35): 355501-355507. [doi:10.1088/0957-4484/19/35/355501]

Link, S., Mohamed, M.B., El-Sayed, M.A., 1999. Simulation of the optical absorption spectra of gold nanorods as a function of their aspect ratio and the effect of the medium dielectric constant. *Journal of Physical Chemistry B*, **103**(16):3073-3077. [doi:10.1021/jp990183f]

Orendorff, C.J., Gearheart, L., Jana, N.R., Murphy, C.J., 2006. Aspect ratio dependence on surface enhanced Raman scattering using silver and gold nanorod substrates. *Physical Chemistry Chemical Physics*, **8**(1):165-170. [doi:10.1039/b512573a]

Oyelere, A.K., Chen, P.C., Huang, X., El-Sayed, I.H., El-Sayed, M.A., 2007. Peptide-conjugated gold nanorods for nuclear targeting. *Bioconjugate Chemistry*, **18**(5): 1490-1497. [doi:10.1021/bc070132i]

Pastoriza-Santos, I., Perez-Juste, J., Liz-Marzan, L.M., 2006. Silica-coating and hydrophobation of CTAB-stabilized gold nanorods. *Chemistry of Materials*, **18**(10):2465-2467. [doi:10.1021/cm060293g]

Perez-Juste, J., Pastoriza-Santos, I., Liz-Marzan, L.M., Mulvaney, P., 2005. Gold nanorods: synthesis, characterization and applications. *Coordination Chemistry Reviews*, **249**(17-18):1870-1901. [doi:10.1016/j.ccr.2005.01.030]

von Maltzahn, G., Centrone, A., Park, J., Ramanathan, R., Sailor, M.J., Hatton, T.A., Bhatia, S.N., 2009. SERS-coded gold nanorods as a multifunctional platform for densely multiplexed near-infrared imaging and photothermal heating. *Advanced Materials*, **21**(31):3175-3180. [doi:10.1002/adma.200803464]

Yu, C., Nakshatri, H., Irudayaraj, J., 2007a. Identity profiling of cell surface markers by multiplex gold nanorod probes. *Nano Letters*, **7**(8):2300-2306. [doi:10.1021/nl070894m]

Yu, C., Varghese, L., Irudayaraj, J., 2007b. Surface modification of cetyltrimethylammonium bromide-capped gold nanorods to make molecular probes. *Langmuir*, **23**(17): 9114-9119. [doi:10.1021/la701111e]